PHYSOR 2016 – Unifying Theory and Experiments in the 21st Century
Sun Valley Resort, Sun Valley, Idaho, USA, May 1 – 5, 2016, on CD-ROM (2016)

INTEGRATED DECAY SOURCE CAPABILITY FOR LARGE-SCALE MONTE CARLO RADIATION TRANSPORT CALCULATIONS

David P. Griesheimer, Stephen C. Marin
Bettis Atomic Power Laboratory
Bechtel Marine Propulsion Corporation, West Mifflin, Pennsylvania, USA
david.griesheimer@unnpp.gov
stephen.marin@unnpp.gov

Paul K. Romano*, Mark H. Stedry
Knolls Atomic Power Laboratory
Bechtel Marine Propulsion Corporation, Niskayuna, New York, USA
mark.stedry@unnpp.gov

ABSTRACT

This paper presents a methodology for sampling neutron and photon decay radiation from radioactive nuclides in continuous-energy Monte Carlo radiation transport calculations. The proposed method uses composition information from the Monte Carlo model description along with ENDF-format decay data to accurately account for the spatial and energy distribution of the source radiation. The method is able to handle models containing many radioactive nuclides distributed among large numbers of unique compositions, such as a depleting 3-D model of a nuclear reactor. A description of the data processing and sampling algorithms associated with the method is presented along with numerical results for several radiation shielding and decay heating problems that are representative of common real-world applications.

Key Words: **Monte Carlo, radiation transport, decay, decay heat**

1. INTRODUCTION

Fixed-source radiation transport analyses often use a source term based on the decay of radioactive nuclides within the system under consideration. For example, in a shutdown or zero-power reactor, calculations for shielding, detector response, startup source, and residual (decay) heat are all driven by the decay of activation and fission products within the reactor. As a result, radiation transport solvers must be able to model both the spatial and energy distribution of a decay source in order to achieve an accurate solution for these types of problems.

Due to the continuous-energy nature of the method, Monte Carlo (MC) simulations are often used for high-fidelity transport calculations involving a decay source. Unfortunately, many widely-used MC transport codes, such as MCNP, require the spatial and energy distribution of the decay source be provided as input to the code as a user-defined source definition. Although many different scripts and helper codes have been developed to assist with generating decay source definitions, the process

* Current affiliation: Argonne National Laboratory, paul.k.romano@anl.gov

often remains tedious and cumbersome, especially for complex decay source terms such as those found in a nuclear reactor. Other MC transport codes such as Geant4 [1] and FLUKA [2] include built-in decay energy spectra for many radioactive nuclides based off of ENSDF [3] data. However, the decay source capability of these codes appears to be targeted towards localized activation/decay calculations rather than large-scale reactor calculations where nuclide inventories change over time-scales that range from seconds to decades.

In this paper we describe a new integrated method for computing and sampling from decay source distributions in large and/or geometrically complex models, such as a 3-D model of a nuclear reactor. The proposed method is designed and optimized to efficiently handle problems with many radioactive nuclides distributed among large numbers of unique compositions, and it uses a fully-integrated approach that does not require any auxiliary input to define the decay source. Instead, nuclide-dependent decay rates, energy release rates, mode branching fractions, and the energy spectrum for emitted neutron and photon radiation are all taken from ENDF-format decay libraries. In addition, the spatial distribution of the decay source is automatically computed from the local nuclide inventories in each cell of the problem. As a result, the decay source automatically updates to account for concentration changes due to depletion/activation or other feedback effects that affect material compositions within the problem. For MC codes with depletion capability, the new method enables the calculation of decay heat and residual radiation levels at different times-in-life using depleted inventories from existing lifetime depletion calculation(s).

2. DECAY DATA FORMAT AND PROCESSING

The amount and quality of decay data included in evaluations such as ENDF [4] and JEFF [5] has improved significantly over the years. For example, ENDF/B VI.1 only included decay data for 979 nuclides when it was released in 1991 [6], while ENDF/B VII.1 currently includes decay data for 3817 nuclides [7], with detailed neutron and/or photon emission spectra provided for decay modes in 1988 of the nuclides. Similarly, JEFF-3.1.1 includes decay data for 3852 nuclides, with detailed emission spectra for 1521 of the nuclides [8].

In the ENDF format, decay data is given in sub-library 4, File 8, MT=457, and includes information on a variety of different decay modes (β^-, electron capture/β^+, internal transition, spontaneous fission, etc.) and different secondary radiations emitted from decay (gamma rays, x-rays, neutron, alpha, etc.). In ENDF/B-VII.1, spontaneous-fission neutron yield data is provided in sub-library 5, File 8, and detailed secondary neutron spectra are given in sub-library 4, File 5, where available (currently only ^{252}Cf has detailed spectral information in ENDF/B-VII.1). In JEFF-3.1.1, spontaneous fission yields and emission spectra for both neutrons and photons are given with other decay data in sub-library 4, File 8, MT=457. Energy distributions for secondary radiation emitted during the decay can be specified using a continuous format, discrete format, or both.

As with other types of nuclear data, it is beneficial to process the raw ENDF-format decay data into a more convenient form. In this implementation, the energy distributions for emitted radiation are converted to a standard ACE LAW 4 representation, which is widely used for secondary energy distributions. In addition to the conversion of the secondary energy distributions, the raw ENDF-format decay data was reorganized to facilitate random sampling during the Monte Carlo simulation.

For each nuclide i, basic data such as the decay constant (λ_i) and the number of decay modes (M_i) is provided, along with detailed information for each decay mode, including: the mode branching fraction ($\beta_{i,m}$), yield by radiation type ($y_{t,i,m}$, where t is the radiation type, neutron or photon), and the secondary energy distribution data for each radiation type. Additional processing is performed to compute the number of decay modes that release each radiation type ($M_{t,i}$), the average yield by radiation type ($y_{t,i}$), and the average energy release by radiation type ($Q_{t,i}$). During processing, energy release values associated with charged particles are lumped together into a single local energy deposition value (Q_{local}). Separating yield and energy release values into neutron, photon, and local categories makes it easier to sample decay mode based on a requested type of radiation and also to integrate the energy released during decay into a general energy deposition framework [9].

Although the ENDF-format defines a standard representation for decay data, there are several ambiguities that must be resolved when using decay data to sample intrinsic radiation sources in a Monte Carlo simulation. One such issue arises when accounting for the presence of compound decay modes that emit multiple types of radiation in a single calculation – e.g., (β^-, neutron)) – or decay modes which have a variable yield of secondary radiation emitted per decay. In these cases, the ENDF-format appears to specify that a single emission spectrum should be defined for each radiation type/decay mode combination. For example, a nuclide with both β^- and (β^-, neutron) decay modes should include a single spectrum each for gamma rays, x-rays, and neutrons. However, in reality, the gamma ray spectrum for the (β^-, neutron) decay sequence is distinct from the β^- decay path without neutron emission. In some JEFF 3.1.1 decay data sets it appears that the evaluators have attempted to provide separate emission spectra for distinct decay sequences related to a single initiating decay mode. For these nuclides, it is possible to separate decay modes with multiple emission yields into distinct decay modes each with a corresponding branching fraction and secondary spectrum. For, example, β^- decay with the possibility of secondary neutron emission can be split into (β^-, 0 neutron), (β^-, 1 neutron), (β^-, 2 neutron) decay modes, etc. While this potentially provides additional fidelity when sampling from the decay emission spectrum, and also allows for decay radiation from certain types of reactions (including compound decays) to be selectively included or filtered out of a source definition, this level of detail is not available in the emission spectrum data for most nuclides.

Another issue when processing raw decay data for use in source sampling and decay heating calculations is ensuring conservation of energy. Each decay data set provides information about total energy release and energy release for several broad categories of radiation types. For most nuclides, decay energy release values are given for electromagnetic, heavy-particle, and light-particle emission categories. However, in some cases the provided energy release information does not agree with the average energy release computed from the secondary emission spectrum data in the evaluation. In these cases, the energy release values must be renormalized to ensure that energy balance is preserved. A recommended strategy is to use the average energy release values computed from the provided emission spectrum data where available, and adjust the local (charged-particle) energy deposition values as needed so that the total decay Q value for each nuclide is preserved.

Finally, the quality of decay data must be carefully considered, especially for extremely short-lived nuclides. A cursory inspection of both ENDF/B-VII.1 and JEFF.3.1.1 decay data suggests that some of the data sets are incomplete or inconsistent with other references. One particular issue of note is

that the ENDF/B-VII.1 evaluation appears to use continuous spectrum representations for ~30 nuclides (including significant decay modes such as delayed neutron emission from ^{87}Br) for which discrete decay data is available. Furthermore, the continuous spectra used for these nuclides in the ENDF/B-VII.1 evaluation do not appear to be consistent with reference values for the spectra available in independent sources such as ENSDF [3] and the Table of Isotopes [10]. By contrast, the JEFF 3.1.1 evaluation only includes continuous spectrum data for decay modes for which discrete data is not available, such as decay modes with multi-body emission (e.g., spontaneous fission) and decay modes where the emission spectrum is based solely on theoretical predictions with no experimental measurement support. Another significant issue is that ENDF/B-VII.1 only includes spontaneous fission neutron spectra for one nuclide (^{252}Cf) and does not provide spontaneous fission photon spectra for any nuclides, whereas JEFF 3.1.1 provides spontaneous fission neutron and photon emission spectra for most transuranic nuclides.

3. DECAY RADIATION SAMPLING ALGORITHM

During MC transport, the initial position, energy, and direction of decay radiation is sampled using information on the relative concentrations of radioactive nuclides throughout the problem, as well as the decay properties for each radionuclide. The decay source algorithm uses a sequential approach for sampling the decay-radiation state information based on conditional probabilities.

The source sampling algorithm begins by computing the emission rate for each distinct type of radiation (neutron, photon, alpha, etc.) due to radioactive decay. Assuming radionuclides are distributed among C independent material compositions, the radiation-dependent emission rate (particles/sec) for each composition c is given by

$$A_{t,c} = V_c \cdot \sum_{i=1}^{M_c} N_{c,i}\, \lambda_i\, y_{t,i}, \tag{1}$$

where V_c is the volume of the composition, M_c is the number of radionuclides in the composition, $N_{c,i}$ is the number density (atoms/cc) of isotope i in the composition, λ_i is the decay constant for nuclide i, and $y_{t,i}$ is the production rate of radiation type t per decay of nuclide i. Note that $A_{t,c}$ can be pre-calculated for all compositions and radiation types prior to particle transport and stored for subsequent use during in-line source sampling. However, in depleting models, the stored values for $A_{t,c}$ must be re-calculated whenever nuclide densities are changed.

Summing $A_{t,c}$ over all compositions c gives the total decay emission rate for each distinct type of radiation, denoted A_t. Similarly, summing A_t over all radiation types gives the total emission rate (in particles/second) for the decay source, denoted A_{total}. Normalizing A_t by A_{total} gives the relative probability that a decay source particle will be emitted with radiation type t,

$$p_t = \frac{A_t}{A_{\text{total}}} = \frac{\sum_{c'=1}^{C} A_{t,c'}}{\sum_{t}\sum_{c'=1}^{C} A_{t,c'}}. \tag{2}$$

During source sampling, a uniformly distributed random number is first drawn to determine the radiation type for each source particle based on the relative probabilities defined by Eq. (2). Note that, in cases where decay sources are combined with other external (fixed) sources, an additional prior sampling step is required to determine which source the particle was emitted from (decay or external). In this situation, the relative probability for each source is given by the corresponding emission intensity for the source divided by the total emission intensity for all sources included in the simulation.

Once the radiation type for a source particle has been selected, the birth location is determined using a rejection sampling technique. Candidate birth coordinates are sampled from a uniform volumetric distribution that covers all compositions containing radioactive nuclides. The composition identifier for the candidate locations is determined and used to calculate (or look up) the decay emission rate of the composition for the given particle radiation type. Sampled locations that fall outside of the model geometry or in a region where the composition decay emission rate is zero are rejected and a new candidate location is re-sampled.

After a candidate birth site in a valid radioactive composition has been sampled, the relative probability that a decay source particle for the source would be produced in this composition is calculated based on the relative activity of the sampled composition against all other compositions in the problem. The relative activity for a composition is computed as the activity density (decays/second-cm^3) of the sampled composition divided by the maximum activity density for any composition in the problem. The sampled birth location/composition is then randomly accepted with probability equal to the relative activity for the composition. Rejected birth locations are resampled from the source volume as before.

Candidate birth sites produced by the previous rejection sampling step are distributed in proportion to composition volume instead of the relative decay emission rate by composition. Therefore, the number of samples in each composition is biased by a factor equal to the ratio of the relative volume fraction to the relative decay emission rate fraction for the composition

$$b_{t,c} = \left(\frac{V_c}{\sum_{c'=1}^{C} V_{c'}} \right) \Bigg/ \left(\frac{A_{t,c}}{\sum_{c'=1}^{C} A_{t,c'}} \right) = \left(\frac{\sum_{c'=1}^{C} A_{t,c'}}{\sum_{c'=1}^{C} V_{c'}} \right) \Bigg/ \left(\frac{A_{t,c}}{V_c} \right). \tag{3}$$

Rearranging factors in Eq. (3) shows that the bias factor for a composition *c* is equal to the ratio of the average decay emission rate density over all compositions to the decay emission rate density for composition *c*. In order to account for the spatial source sampling bias, the birth weight of each

candidate particle must be adjusted by a factor of $1/b_{t,c}$. If desired, unbiased weight adjustment games such as splitting and Russian roulette can then be applied to restore the desired initial source particle weight by replicating overweight particles and randomly killing underweight particles. Alternatively, candidate source particle locations can be rejected and resampled with probability

$$p_{t,c}^{\text{reject}} = 1 - \frac{A_{t,c}/V_c}{\max_{c'}\left(A_{t,c'}/V_{c'}\right)}, \tag{4}$$

where $\max\left(A_{t,c'}/V_{c'}\right)$ is the maximum decay emission rate density over all compositions. Note that this technique is simply a variation of the general weight adjustment strategy, in which all source particle weights are scaled by a factor of $1/\max\left(A_{t,c'}/V_{c'}\right)$ to prevent splitting, and re-sampling is used to replace particles terminated by roulette (instead of increasing the weight of surviving particles). The on-the-fly rejection/resampling technique is especially easy to implement and produces unbiased sample populations of equal-weight source particles.

Once a birth location has been accepted, the parent nuclide for the source particle is sampled in proportion to the relative emission rate for each nuclide in the sampled composition. The relative probability that radiation of type t is emitted from nuclide i in composition c is given by

$$p_{t,i} = \frac{N_{c,i}\,\lambda_i\,y_{t,i}}{\sum_{i'=1}^{M_c} N_{c,i'}\,\lambda_{i'}\,y_{t,i'}}. \tag{5}$$

After the parent decay nuclide has been sampled, the decay mode for the source particle is sampled in proportion to the relative emission rate for each decay mode that emits the given radiation type. The relative probability that radiation of type t is emitted from decay mode m of nuclide i in composition c is given by

$$p_{t,m} = \frac{y_{t,i,m}}{\sum_{m'=1}^{M_i} y_{t,i,m'}}. \tag{5}$$

Note that $y_{t,i,m}$ is the decay yield for nuclide i, decay mode m, radiation type t, and that the yield value includes the branching fraction for the corresponding nuclide/decay mode combination.

Finally, once the location, nuclide, and decay mode have been determined, the birth energy and direction for the source particle are set. The birth energy of the particle is sampled from the LAW 4 secondary energy distribution associated with the radiation type and decay mode, typically using the same sampling routines used for all other scattering and secondary particle generation operations in the MC code. The direction of the source particle is sampled from an isotropic distribution.

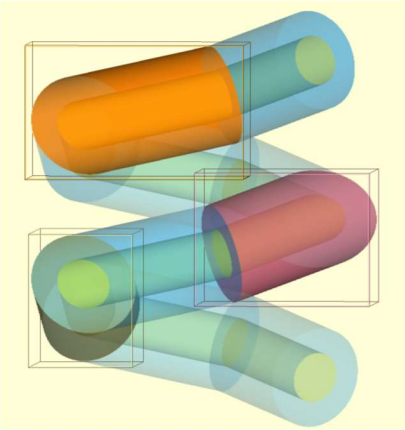

Figure 1. Helical pipe formed from 10 pairs of nested cylinders. The outer diameter of the pipe is 4 cm, including a 1 cm thick carbon steel wall. The interior of the pipe is filled with neutron-activated water with 3.5×10^{6} Bq/cm^3 of ^{16}N and 150 Bq/cm^3 of ^{17}N.

The algorithm described above can be adapted to only sample one certain type of radiation (e.g., neutron or photon) or to sample only radiation emitted from a particular set of nuclides and/or decay modes. This capability is especially useful for conducting sensitivity studies or to improve efficiency when one particular nuclide or mode is known to dominate the decay source.

4. NUMERICAL RESULTS

The integrated decay source capability was implemented in a developmental version of MC21 [11], an in-house continuous-energy MC radiation transport code. Processing of the raw ENDF-format decay data as described in Section 2 was performed by NDEX [11], an in-house code for creating continuous-energy cross sections for MC21. In order to demonstrate the flexibility and ease-of-use of the new method, two types of realistic example calculations involving decay sources are presented.

4.1. Activated Coolant Pipe Shielding Example

The first example considers the radiation field from the decay of ^{16}N and ^{17}N in water that has been irradiated by neutrons, which is a common type of shielding calculation for water-moderated/cooled reactors. The problem includes a 4 cm diameter carbon-steel pipe (1 cm wall thickness) that is filled with water. In addition to hydrogen and oxygen, the water in the pipe contains trace amounts of ^{16}N and ^{17}N that produce decay activity levels of 3.5×10^{6} Bq/cm^3 and 150 Bq/cm^3, respectively, which is similar to activity levels seen in commercial nuclear power plants. The pipe geometry uses 10 pairs of nested cylindrical components to approximate a helical shape with two full turns, as shown in Figure 1. The overall dimensions of the helical pipe are approximately 14 cm × 14 cm × 13 cm.

The complex geometry of this piping arrangement makes it tedious to manually define a volumetric decay source distribution for this model. However, with an integrated decay source capability the radioactive nuclides are simply added to the water material definition and the problem can be run without any other input. Figure 2 shows photon radiation flux results taken over the axial and radial

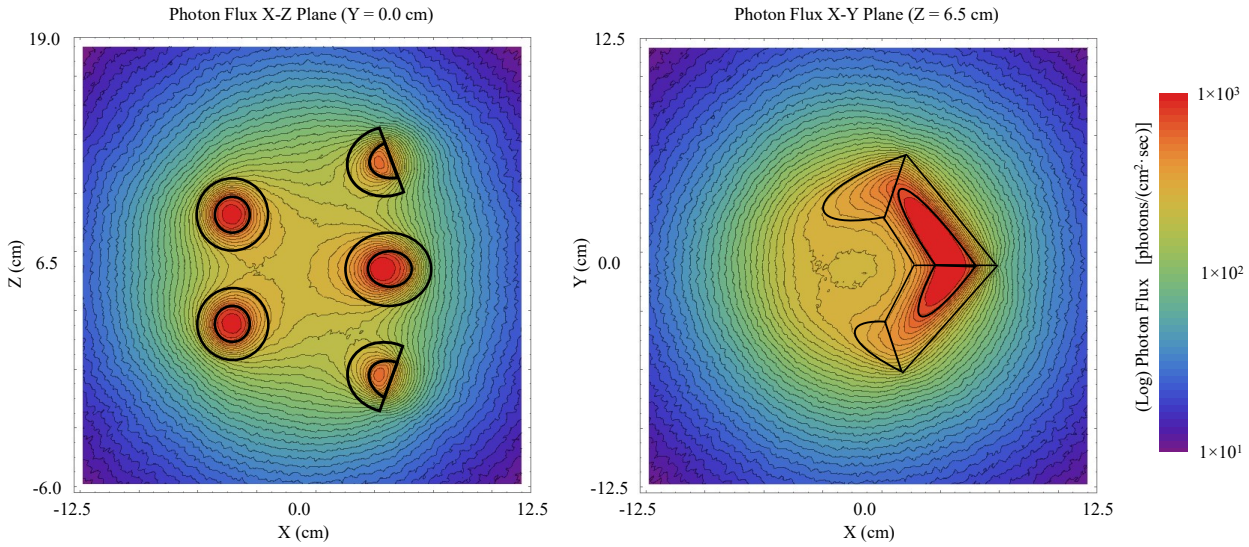

Figure 2. Photon flux resulting from decay of ^{16}N in a helical pipe. Images show the photon flux in the axial (*x*-*z*) and radial (*x*-*y*) cross section planes for the pipe. The black lines on the plots indicate the outline of the pipe wall.

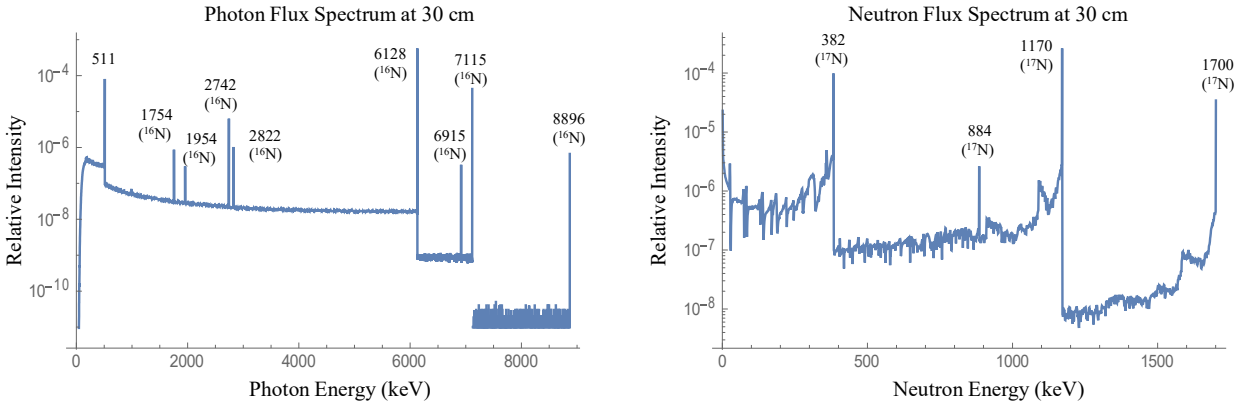

Figure 3. Energy spectrum in 1 keV bins for neutron and photon flux at a distance 30 cm from the helical pipe. Primary decay energies for ^{16}N and ^{17}N are identified on the plots.

cross section of the pipe at the centerline of the helix for a fixed-source MC21 calculation with 1×10^8 source histories and using ENDF/B-VII.1 cross sections and decay data. This figure clearly shows the decay source in the interior of the pipe, followed by material attenuation through the pipe wall and geometric attenuation as the radiation moves though air away from the pipe. Figure 3 shows the neutron and photon flux spectrum for escaping radiation taken over a 30 cm sphere centered on the pipe. Note that the resulting spectra clearly show the photon and neutron emission peaks that correspond to ^{16}N and ^{17}N.

4.2. PWR Decay Heating Example

The second example focuses on the calculation of decay heat following shutdown of a nuclear reactor. Decay heating calculations are important for reactor safety analyses, as well as for calculations in support of the handling, transportation, storage, and disposal of spent nuclear fuel. As an initial test of the in-line decay source/heating capability, MC21 was used to calculate the decay power of a pressurized water reactor (PWR) unit-cell (pin-cell) as a function of irradiation time and shutdown time. The unit-cell model is based on a fuel element specification for the H.B. Robinson reactor, obtained from Reference 12. The modeled fuel element includes a 0.93 cm diameter cylindrical pellet of 2.56% enriched UO_2, surrounded by a 0.01 cm air gap and 0.06 cm of Zircaloy-4 cladding, for a total element diameter of 1.07 cm. The fuel element is located in the center of a water-filled parallelepiped with radial dimensions (length and width) of 1.43 cm and height of 1.0 cm. Reflecting boundary conditions are applied to all surfaces of the parallelepiped to simulate an infinite square lattice of fuel pins with zero axial leakage. The water surrounding the fuel element was modeled as H-H_2O, O16, and ~160 ppm soluble boron with density corresponding to conditions at 2250 psia and 520°F. Isothermal 520°F ENDF/B-VII.0 cross section data and JEFF-3.1.1 decay data was used for all nuclides.

The pin cell was depleted at a power density of 30 MW/MTU for periods of 1 second to 10,000 hours (1.14 years) using the built-in depletion solver in MC21. Reaction rates for each depletion calculation were obtained from an eigenvalue neutron transport calculation with 120 batches (20 discarded) of 15,000 neutron histories. Depletion calculations less than 1,000 hours at-power used a single constant-flux depletion step to calculate the end-of-timestep nuclide number densities. The 1,000 and 10,000 hour at-power calculations used a multi-step predictor-corrector depletion calculation, with 1 and 2 corrector steps, respectively. Following the at-power depletion step, a set of nine zero-power depletion calculations were performed to obtain the nuclide number densities at times ranging from 0.1 seconds to 1×10^8 seconds (3.17 years) after shutdown. For each shutdown time, decay heating rates were calculated and reported by MC21, based on the depleted nuclide inventories and corresponding decay data (decay rate and energy release per decay) for each nuclide. All calculations were performed on 28 Intel Xeon Sandy Bridge 8-core processors (224 cores total) running at 2.6 GHz. Average run time for the constant-flux calculations was 4.25 minutes, including 2.75 minutes to read and initialize nuclear data, 1.25 minutes for the radiation transport calculation, and 0.1-0.2 seconds for each depletion calculation.

During each depletion calculation, a backwards-differentiation-formula (BDF) numerical solver was used to determine updated concentrations for 1351 unique nuclides (1303 fission products and 48 actinides). Of these 1351 depletable nuclides, 1169 nuclides have cross section and/or depletion data available and are explicitly included in the MC21 material definition for the UO_2 fuel. The remaining 182 nuclides are only included in the system of coupled depletion equations as precursor nuclides to ensure that all transmutation and decay paths are modeled accurately.

The calculated decay heating results from MC21 are shown in Figure 4, along with corresponding values from an empirical decay heat correlation taken from Todreas and Kazimi [13]. Note that the heating values from both MC21 and the empirical correlation include energy release from the decay of fission product and capture (activation) product nuclides. Inspection of Figure 4 shows that the

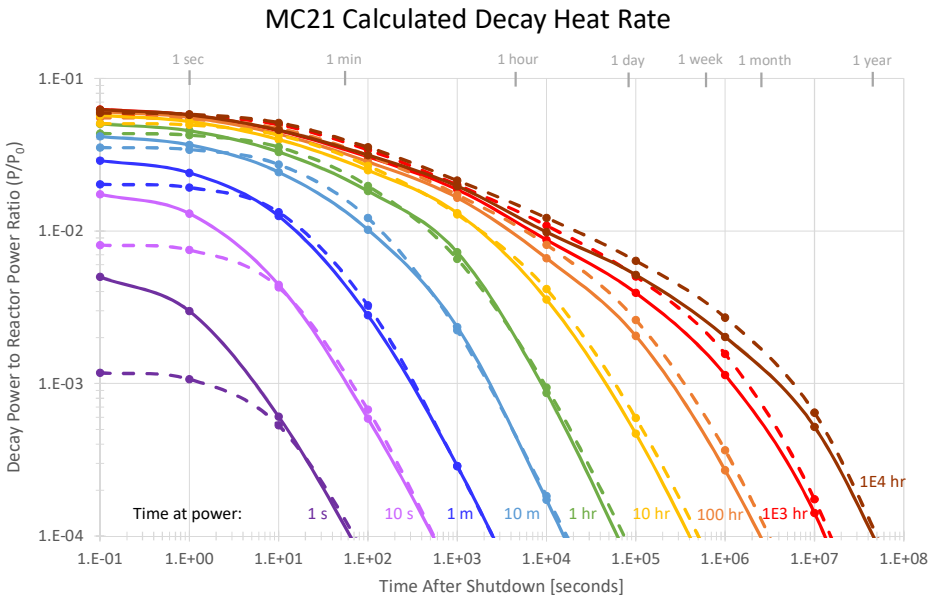

Figure 4. Decay heat rates for a PWR pin cell, shown as a function of irradiation time and shutdown time. Solid lines show results from MC21 in-line decay heating calculations using 1169 explicit nuclides. Dashed lines show results from an empirical decay heat correlation given in Todreas and Kazimi [13].

MC21 results agree well with the reference decay heating curves for shutdown times > 10 seconds for all at-power intervals. For shutdown times less than 2-3 seconds, the MC21 results are consistently larger than the empirical results, with significant over predictions of 2-4× for at-power intervals less than 1 minute. The reason for these differences at small shutdown times and power intervals is not understood at this time.

Additional testing showed that the accuracy of decay heat estimates from MC21 degraded quickly when the number of nuclides included in the model was decreased. For example, when the number of nuclides was reduced from 1169 to 277, the decay heating rate calculated by MC21 was 8-11 times smaller than the reference value for shutdown times less than 2 minutes. However, agreement improved to less than a 10% under-prediction at 2 weeks following shutdown, suggesting that reduced-order depletion systems containing fewer explicitly-represented nuclides may produce reasonable decay heating estimates for transportation and repository calculations months to years after shutdown. For short shutdown times, it may also be possible to reduce the number of nuclides explicitly-represented in the MC model by combining nuclides with similar decay half-lives into effective decay heating groups, similar to what is done for delayed neutron precursors in transient calculations.

For a more realistic test, MC21 was used to calculate local decay heating rates in a 3-D, eighth-core, PWR model. The core model includes 47 fuel assemblies configured in a typical PWR arrangement with quarter-core radial symmetry and half-core axial symmetry. All fuel assemblies in the core were assumed to have identical geometry and initial compositions at beginning-of-life. Each assembly consists of a 15×15 lattice of cylindrical rods, including 204 fuel elements, 12 burnable absorber

rods, and 9 control rod guide tubes. The geometric details of the assembly and constituent fuel, poison, and guide tube elements are based on the specifications for H.B. Robinson assembly B05, provided in Reference 12. Fuel assemblies in the $1/8^{th}$ core model are 207.88 cm high, including 182.88 cm of active fuel and a 25 cm water reflector region at the top of the core. Each of the 10,152 fuel and poison elements were subdivided into 19 axial segments for depletion purposes, yielding 192,888 unique depletable compositions in the $1/8^{th}$ core model. As in the previous example, each composition included 1169 depleting nuclides, for a total of 2.254×10^6 depleting nuclides in the model. Total memory usage for the model, including all cross section data, nuclide concentration data, and depletion reaction rate data, was 11.32 GB per compute node. Additional details on the 3-D, eighth-core, model used in this study are provided in Reference 14.

MC21 was used to simulate core depletion through three consecutive operating cycles of 5,844, 5,844, and 3,744 full-power hours, respectively. A constant reactor power level of 328 MW (31.47 MW/MTU) was used during each operating cycle, which corresponds to a total rated power of 2,624 for the full core. Each operating cycle included an initial 100-hour depletion timestep for xenon build-in, followed by 3-5 at-power depletion timesteps of between 944 and 1,244 hours. Following cycles 1, 2, and 3, shutdown periods of 960, 1,536, and 936 hours, respectively, were explicitly modeled using zero-power depletion timesteps in MC21. Each shutdown period was divided into an initial 1-hour depletion timestep, followed by the remaining shutdown interval in a subsequent depletion timestep. The entire three-cycle depletion calculation included 16 at-power and 6 shutdown depletion calculations. Each at-power depletion calculation used a running strategy of 600 batches (including 100 discarded) of 100,000 neutron histories each and ran for approximately 52 minutes (±7 minutes) on 384 Intel Xenon Haswell cores (32 processors × 12 cores) running at 2.5 GHz. Depletion calculations ran for between 33 and 137 seconds on the same number of processors as the at-power radiation transport calculations.

During the simulation, local decay heating rates were collected throughout the core model. Figure 5 shows the decay heating rate at the radial ($z = 0$) and axial ($y = 0$) core mid-planes 1 hour after shutdown for cycles 1-3. Inspection of Figure 4 shows that decay heat density is highly peaked at the center of the core after cycle 1, with a maximum decay heat density of 2.55 W/cm^3. Following cycles 2 and 3, the distribution of decay heat has spread out through the core and moved axially upward as fission density in the center of the core decreases due to fuel depletion. As a result of the spatial redistribution of fission density, the peak decay heating density following cycles 2 and 3 (1.83 W/cm^3 and 1.53 W/cm^3, respectively) is approximately 30-40% lower than after cycle 1, even though the total decay heat produced by the core remains relatively constant at 4.23 MW (± 0.027 MW) after all three cycles.

5. CONCLUSIONS

A new integrated decay source capability for continuous-energy MC radiation transport simulations has been developed and tested on several models that are representative of real-world applications. The new integrated decay source capability uses spatial rejection sampling to generate emission sites for decay radiation based on the nuclide inventories throughout the model. In addition, the energy of the radiation emitted in the decay is sampled from the nuclide- and decay-mode-dependent secondary energy distributions from the ENDF-format decay sub-libraries. As a result, the

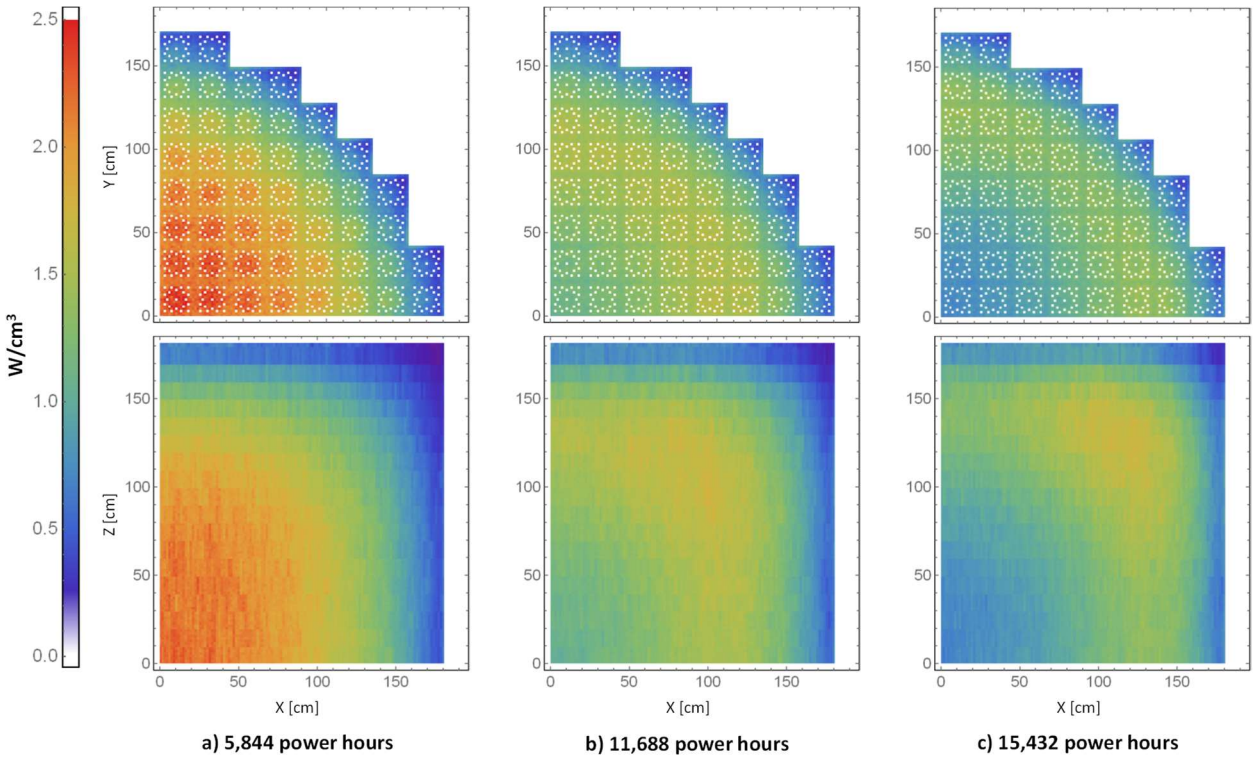

Figure 5. Local decay heat density at radial ($z = 0$) and axial ($y = 0$) mid-plane for a 3-D, eighth core PWR model 1 hour after shutdown following power operations. Results are shown for three consecutive full-power operating cycles of 5,844, 5,844, and 3,744 hours, respectively.

method produces a decay source that is as accurate as the underlying nuclide inventory representation and decay data evaluations. The integrated decay source method eliminates the need to generate decay sources by hand or with an external script, and greatly simplifies the process for performing shielding, spectroscopy, and/or shutdown source calculations using existing MC model geometries.

ACKNOWLEDGMENTS

The authors would like to thank Drs. Jesse Holmes, Mike Zerkle, Hansem Joo, and David Carpenter from the Bettis Laboratory and Drs. Timothy Trumbull and Ed Caro from the Knolls Laboratory for many helpful discussions on physics and data issues related to nuclear decay.

REFERENCES

[1] M. Asai et al., "Recent Developments in Geant4," *Ann. Nucl. Energy*, **82**, pp. 19 – 28 (2015).
[2] G. Battistoni et al., "Overview of the FLUKA Code," *Ann. Nucl. Energy*, **82**, pp. 10 – 18 (2015).
[3] "Evaluated Nuclear Structure Data Files", available online. URL http://www.nndc.bnl.gov/ensdf/ (2015).

[4] M. Herman, A. Trkov, and D.A. Brown, "ENDF-6 Formats Manual," ENDF-102/BNL-90365-2009, Rev. 2, December 2011.
[5] A. Santamarina et al., "The JEFF-3.1.1 Nuclear data Library," JEFF Report 22, Organisation for Economic Co-operation and Development, National Energy Agency (2009).
[6] H.D. Lemmel (ed.), "ENDF/B-6 Decay Data Library," informal report, IAEA-NDS-108, Rev. August 1992 (1992).
[7] "ENDF/B-VII.1 Evaluated Nuclear Data Library," available online. URL http://www.nndc.bnl.gov/endf/b7.1/ (2015).
[8] M.A. Kellett, O. Bersillon, R.W. Mills, "The JEFF-3.1/3.1.1 Radioactive Decay Data and Fission Yields Sub-Libraries," JEFF Report 20, Organisation for Economic Co-operation and Development, National Energy Agency (2009).
[9] D.P. Griesheimer and M.H. Stedry, "A Generalized Framework for In-Line Energy Deposition During Steady-State Monte Carlo Radiation Transport," *Proceedings of the International Conference on Mathematics and Computational Methods Applied to Nuclear Science and Engineering (M&C 2013)*, Sun Valley, Idaho, May 5 – 9, CD-ROM (2013).
[10] R.B. Firestone et al., Table of Isotopes, Eighth Edition, Volume I, Wiley-Interscience, New York, New York (1996).
[11] D.P. Griesheimer et al., "MC21 v.6.0 – A Continuous-Energy Monte Carlo Particle Transport Code with Integrated Reactor Feedback Capabilities," *Ann. Nucl. Energy*, **82**, pp. 29 – 40. DOI: http://dx.doi.org/10.1016/j.anucene.2014.08.020 (2015).
[12] O.W. Hermann, S.M. Bowman, M.C. Brady, and C.V. Parks, "Validation of the SCALE System for PWR Spent Fuel Isotopic Composition Analyses," Oak Ridge National Laboratory, ORNL/TM-12667 (1995).
[13] N.E. Todreas and M.S. Kazimi, Nuclear Systems I: Thermal Hydraulic Fundamentals, Taylor and Francis, New York, New York (1990).
[14] S.J. Spychala and D.P. Griesheimer, "Effects of Stochastic Noise on a Three-Dimensional Monte Carlo Depletion Analysis of the H.B. Robinson Reactor," *Proceedings of PHYSOR-2014 – The Role of Reactor Physics Toward a Sustainable Future*, Kyoto, Japan, September 28 – October 3, CD-ROM (2014).